Proceedings World Geothermal Congress 2020+1
Reykjavik, Iceland, April - October 2021

Thermal-Structural Analysis of an Eroded Casing Section of a Geothermal Production Well with High Total Suspended Solids

Daryl Marc G. On

Energy Development Corporation, One Corporate Centre Building, Ortigas Center, Pasig City, Philippines

on.dmg@energy.com.ph

Keywords: finite element modelling, ANSYS®, thermal-structural, penetrated casing, total suspended solids

ABSTRACT

A finite element model was developed for a 1-meter section of a geothermal production well with high total suspended solids. The modelled section contained an isolated pit which was recorded to be the deepest penetration based on the obtained log data of a casing caliper survey. The penetration was assessed to be the results of the abrasive effects of high-velocity solids that impacted the 9-5/8" reline casing overtime. The structural integrity of this casing section was evaluated by modelling the stresses at flowing condition as well as during quenching and air compression using ANSYS® Academic Teaching Mechanical and CFD, Release 19.1 (ANSYS, Inc., 2018) and determining whether the calculated stresses satisfy the *von Mises* criterion. The obtained results from the numerical modelling showed that a stress concentration has developed at the isolated pit of the 9-5/8" reline casing. At flowing condition, the casing section was evaluated to be generally safe using the *von Mises* criterion. The simulated *von Mises* stress at the isolated pit was found to be 44.85 MPa which is less than the assumed ultimate yield strength of steel at 460 MPa. Identical evaluations were obtained for the quenching and air compression scenarios where the *von Mises* stresses at the isolated pit were calculated to be at 78.22 MPa and 199.49 MPa, respectively. The maximum principal stresses at the isolated pit in both flowing condition and quenching, however, have exceeded the calculated critical burst pressure for the 9-5/8" reline casing at 45.12 MPa. These results indicate that the burst failure of the 9-5/8" reline casing is imminent without the support of the surrounding concretes and outer casings. For the air compression, the principal stresses of the 9-5/8" reline casing were obtained to be compressive suggesting that it has less likelihood of bursting.

1. INTRODUCTION

Tapping heat from geothermal reservoirs through the extraction of reservoir fluids imposes high temperature and pressure loads to production wells. For such condition, a typical production well is designed to have several concentric steel casings that are cemented with each other (Southon, 2005). In addition to these loads, the presence of suspended solids during production can affect the structural integrity of the casings. Steam flow accompanied with high concentrations of suspended solids overtime can lead to casing penetrations. Severe cases of wells with high total suspended solids caused damages not only to the casings but also to branch lines and other surface equipment (Buñing et al., 2005). Wells with such conditions are closely monitored and are installed with solid traps to prevent further damage to surface equipment. However, the casings of these wells are still left vulnerable to the abrasive effects of the high-velocity solids. The casings can also be damaged by corrosion if the fluid flowing in the well have low-pH. Geothermal wells may also undergo intervention activities such as quenching and air compression as part of the management strategy for sustainability. These activities involve changes in pressure and temperature conditions and may further damage casing sections with deteriorated conditions if not carefully planned and executed.

Wells with penetrated casing sections have lower resistance to burst failures due to the reduced casing wall thickness (Bourgoyne et al., 1986). Of interest in this situation are the resulting stresses in the casing, if they are still within the strength limits under operating flowing condition. Further, understanding how these stresses are affected by changes in pressure and temperature loads is of importance. In this study, finite element modelling is used to investigate these questions. This method allows numerical approximation of field problems such as the spatial distribution of stress and temperature (Pidaparti, 2017). With finite element modelling, the structural integrity of penetrated casing sections presumed to be eroded by the abrasive effects of high-velocity solids can be analyzed in different pressure and temperature loads.

Geothermal wells have been numerically simulated previously in the literature to analyze the stresses and strains on the casings induced by pressure and temperature loads. One study aimed to examine the buckling behavior of the production casing of a vertical geothermal well (Magnúsdóttir, 2009). In this study, two-dimensional thermal-structural analyses were first conducted to determine the temperature and stress distribution in the well which served as inputs for the three-dimensional structural analyses of the buckling behavior. Kaldal et al. (2015) also used numerical model to characterize wellhead displacement of geothermal wells due to thermal expansion. In their study, they used transient thermal-structural analyses and validated their results using historical data of measured wellhead displacements. Akbar et al. (2016) focused on fluid flow transient analyses of a high enthalpy geothermal well and presented transition of fluid flow regimes including phase change. Simulated flowing temperature and pressure profiles closely matched the measured data, and the results accurately described the temperature and pressure loads inside the wellbore casing.

This paper aimed to develop a finite element model of a penetrated casing section of a geothermal well under operational flowing condition as a baseline, and to investigate the stresses in the casing during quenching and air compression. The finite element model of the penetrated casing section and the thermal-structural analyses were simulated using ANSYS® Academic Teaching Mechanical and CFD, Release 19.1. Developing the finite element model involved making assumptions to simplify the problem, evaluating the boundary conditions, and establishing the mesh design through convergence test. Note that the baseline model assumed that the isolated pit is already present in the casing section of interest and there were no attempts made to model any erosion or corrosion

On

scenarios that caused this isolated pit to form. The results from the baseline model under operational flowing condition as well as from the models representing the well intervention activities are provided in this paper.

2. NUMERICAL MODEL AND ASSUMPTIONS

The geothermal well considered in this study was recorded to have high concentration of suspended solids which caused damage to the casings and the wellhead assembly. The well is operating at 1.3 MPa wellhead pressure with single phase steam (enthalpy = 2780 kJ/kg) flowing at a rate of 10 kg/s. The well has undergone relining operation down to 802 meters using 9-5/8" casing. A casing caliper inspection survey was conducted to inspect the integrity of the 9-5/8" reline casing using a 30-arm caliper tool after months of continuous utilization. The survey logged interval started from casing head flange down to 120 meters. Results of the caliper survey showed that the deepest penetration is an isolated pit located in the middle of Joint #2 at depth 19.4 meters. This penetration was recorded to be 0.14" or 30% of the casing wall thickness as shown in the cross-section measurement of 30-arm caliper tool in Figure .

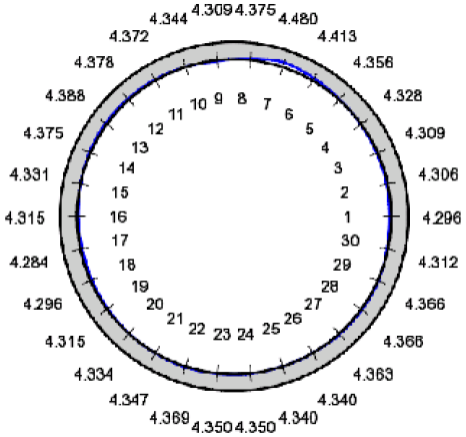

Figure 1: Cross-section measurement in inches of the 30-arm caliper tool at depth 19.4 meters

The models of steel casings and the cement were assigned with structural steel and concrete, respectively. The mechanical and thermal properties of these materials are found in ANSYS® library of engineering data and are summarised in Table 1.

Table 1: Summary of mechanical and thermal properties of structural steel and concrete used in the study (ANSYS, Inc., 2018)

Properties	Structural Steel	Concrete
Density [kg/m^3]	7,850	2,300
Poisson's Ratio	0.3	0.18
Elastic Modulus [GPa]	200	30
Ultimate Tensile Strength [MPa]	460	5
Thermal Expansion Coefficient [1/°C]	1.2E-05	1.4E-05
Thermal Conductivity [W/m °C]	60.5	0.72

2.1 Geometry and Mesh

A 1-meter interval of the casing section which contains the highest penetration at depth 19.4 meters was modelled as shown in Figure 1. The model consisted of three concentric casings (9-5/8" reline casing, 13-3/8" production casing, and 18-5/8" anchor casing) and three concrete bodies that are in contact with each other. The outer diameter of the outermost concrete measured to be 26" based on the size of the drilled hole at that depth. For the 9-5/8" reline casing, the profile of the isolated pit was manually constructed based on the obtained log data of the casing caliper survey. The mesh design of this model consists of tetrahedral, hexagonal, and wedge elements that were generated using automatic meshing method. Body size refinement was applied to the three steel casings and the two inner concrete bodies to accurately capture the simulated stresses. As a good finite element practice, gradual change in element size was maintained to avoid convergence problems (Pidaparti, 2017). This was done by assigning a face size refinement to the inner surface of the outermost concrete body. Since the outermost concrete body is of less interest, its outer surface was also assigned a face size refinement at 2.25 times the size of the elements of the inner bodies.

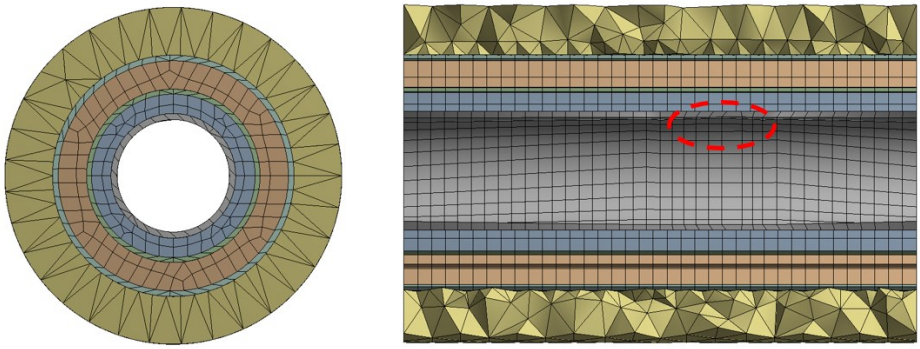

Figure 1: Mesh design of the casing section: top view (left), cross-section view highlighting the isolated pit (right)

2.2 Boundary Conditions

Sliding between the steel casing and the cement occurs in reality which results to wellhead displacement. This problem can be modelled using nonlinear frictional contact to yield an accurate solution as demonstrated in the literature (Kaldal et al., 2015). However, this is more computationally demanding due to the finer mesh requirement to model the contact nonlinearity behavior. Frictional contact was tested initially using a fine mesh design close to the node and element limitation of the ANSYS® Academic Version, but the simulation runs failed to attain convergence. Since the section of interest is only a 1-meter interval containing the isolated pit, the sliding between the contact faces of the steel casing and the cement was assumed to be negligible and the contact type was set to bonded.

When thermal loads are considered, constraining the outer surface boundary via fixed support restricts the nodes artificially resulting to large unrealistic stresses. This can be eliminated by applying elastic support at the surface boundary to allow for node displacement (Barrett, 2015). This type of support was applied at the outer surface of the outermost concrete along with a foundation stiffness value of 27,440 Pa/m to represent the surrounding rock as suggested by Pagli et al. (2007) in their model. The bottom surface of the model was assigned a frictionless support to constrain the nodes from moving downwards the axial direction. Given the dry output of the well, the flowing pressure and temperature profiles along the entire well track are nearly isobaric and isothermal, respectively. A pressure load of 1.3 MPa based on the operating wellhead pressure, along with the corresponding saturation temperature of 191.6 °C, were assigned to the inner surface of the 9-5/8" reline casing.

2.3 Convergence Test

Convergence test was conducted to check the balance between numerical accuracy and computational time requirement of the simulations. This was done using the h-method wherein the characteristic length *h* of elements is decreased resulting in a finer mesh density while maintaining the element type (Kurowski, 2002). The input parameters for the convergence test are the element sizes at the different aforementioned refinements. Mesh densities ranging from 10,000 to 70,000 elements were tested by adjusting the values of input parameters and these are summarized in Table 2. Using similar boundary conditions, six iterations were solved to examine the effect of refinement on the simulated *von Mises* stress at the midpoint of the isolated pit and the vertical deformation at the upper end of the 9-5/8" reline casing.

Table 2: Summary of element sizing parameters used in the convergence test

Body Sizing of the 3 casings and the inner and middle concretes [mm]	Face Sizing at inner surface of outer concrete [mm]	Face Sizing at outer surface of outer concrete [mm]	Number of Elements
32	32	72	10359
30	30	67.5	20711
28	28	63	25148
24	24	54	37455
20	20	45	51750
18	18	40.5	62800

The simulated *von Mises* stress and deformation values were plotted with their corresponding number of elements as shown in Figure 2. While no significant differences were observed in the deformation for the six iterations, the *von Mises* stress started to stabilise at ~25,000 elements. This means that no further significant accuracy can be attained by increasing the mesh density beyond this point, thus a mesh consisting of 25,148 elements was used in the analyses.

On

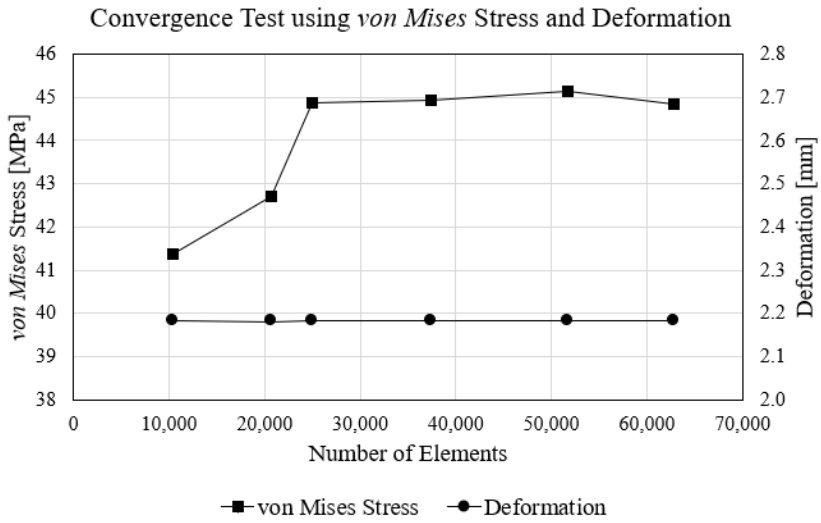

Figure 2: Convergence test using *von Mises* stress and deformation

3. RESULTS AND DISCUSSION

The simulation for the baseline model at operational flowing condition was carried out by performing a steady state thermal analysis and then importing the simulated temperature as a thermal load to the static structural analysis. The simulated temperature at 191.6 °C is uniformly distributed across the model at a steady state condition as shown in Figure 3.

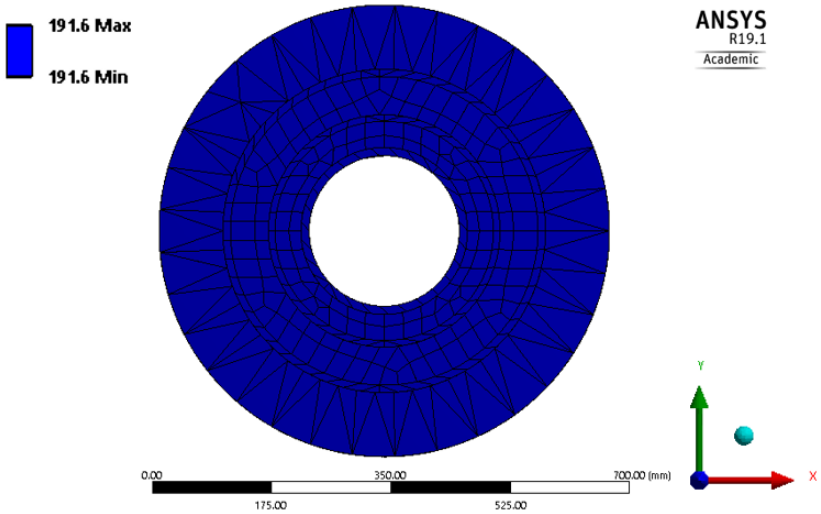

Figure 3: Simulated temperature of the baseline model at flowing condition

Applying the combined effects of thermal and mechanical loads for the static structural analysis, the resulting *von Mises* stress distribution of the model is illustrated in Figure 4. The *von Mises* stress is used as a failure criterion for isotropic ductile materials and is defined as a function of the principal stresses as shown in Equation 1. This failure criterion states that an isotropic ductile material is safe from yielding if its equivalent *von Mises* stress is less than or equal to the yield strength (Christensen, 2013).

$$\sigma_e = \left[\frac{(\sigma_1 - \sigma_2)^2 + (\sigma_2 - \sigma_3)^2 + (\sigma_3 - \sigma_1)^2}{2}\right]^{1/2} \leq \sigma_Y \quad (1)$$

where σ_e = *von Mises* stress, $\sigma_1, \sigma_2, \sigma_3$ = principal stresses, and σ_Y = yield strength

Looking at the *von Mises* stress distribution in Figure 4, the simulated stress values are way below the assumed ultimate tensile strength of the steel at 460 MPa. This indicates that the casing section is safe based on the *von Mises* criterion. The isolated pit of the 9-5/8" reline casing has a stress value of 44.85 MPa at its midpoint while the immediate region surrounding the isolated pit has a value of around 35 MPa. The regions of the 9-5/8" reline casing that are farther from the isolated pit have lower stress values. This indicates that the alteration of the casing due to penetration resulted to stress concentration. Surprisingly, the 13-3/8" production casing and the 18-5/8" anchor casing have higher stress values than the 9-5/8" reline casing although their stress distributions are more gradual in the absence of the stress concentration due to penetration. The highest *von Mises* stress is found at the 18-5/8" anchor casing at a value of 55.49 MPa. In addition, the stresses at the upper end of the model are lower than those at the bottom because of the free displacement of nodes. For the concrete bodies, the simulated *von Mises* stress are generally low at around 2.45 MPa which is also less than the assumed ultimate tensile strength at 5 MPa. Note, however, that the *von Mises* criterion does not apply to brittle material such as concrete hence this may not necessarily mean that the cement failure will not happen.

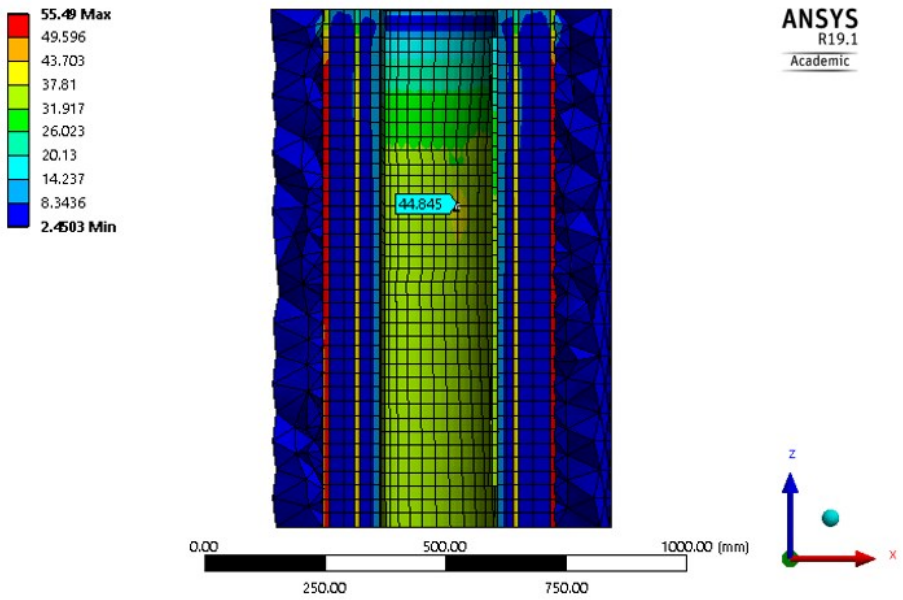

Figure 4: Cross-section of the baseline model showing the *von Mises* stress distribution in MPa unit at flowing condition

The burst failure of well casings can be assessed by solving the critical pressure value as expressed in Equation (2) (Bourgoyne et al., 1986). The critical value of burst pressure is a function of material strength, casing wall thickness, and casing diameter. A burst failure can be expected when the critical value is exceeded by the stresses in the casing.

$$P_b = \frac{2\sigma t}{d} \tag{2}$$

where P_b = burst pressure, σ = yield strength, t = thickness, d = casing diameter

The critical value of burst pressure as described in Equation (2) is equivalent to the hoop stress of a thin-walled cylindrical pressure vessel. Applying axisymmetry, the hoop stress is the maximum principal stress of the casing. The corresponding critical burst pressure value of the 9-5/8" reline casing is 45.12 MPa given a wall thickness of 11.2 mm and an assumed ultimate yield strength of steel at 460 MPa. By considering the reduction in wall thickness due to penetration, the critical value of burst pressure will be lower. The critical burst pressure is then compared to the simulated maximum principal stress of the baseline model as shown in Figure 5. At the midpoint of the isolated pit, the maximum principal stress has a value of 46.6 MPa which is slightly higher than the critical burst pressure. This may indicate that burst failure of the 9-5/8" reline casing is imminent without the support of the surrounding concretes and outer casings. Similar contour is observed with the maximum principal stress distribution when compared to *von Mises* stress distribution. The 13-3/8" production casing and the 18-5/8" anchor casing have higher stress magnitudes while the concrete bodies have lower values. The critical values of burst pressure of the 13-3/8" production casing and the 18-5/8" anchor casing are also computed at 26.13 MPa and 21.47 MPa, respectively. The simulated maximum principal stresses at the outer casings have exceeded these critical values. It is important to note, however, that these simulated stresses were obtained using a bonded contact type among the different casing and concrete bodies. Sliding in between contacting bodies is not allowed in this contact type which resulted to such high stress values. The stresses on the outer casings can be more accurately solved by considering nonlinear contact types such as friction as previously discussed in the boundary conditions.

On

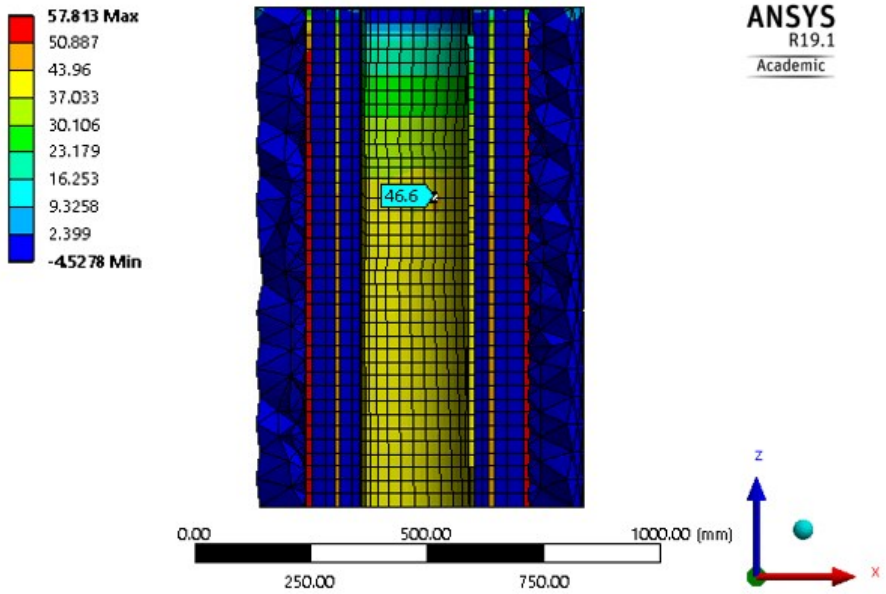

Figure 5: Cross-section of the baseline model showing the maximum principal stress distribution in MPa unit at flowing condition

The simulated total and vertical deformations of the casing section as a result of the combined effect of thermal and mechanical loads are shown in Figure 6. As observed in these contours, the major component of the total displacement is in the vertical direction with the upper end having the most displacement. Using thermal expansion coefficient 1.2E-05 $°C^{-1}$ of structural steel and an initial temperature of 22 °C, the theoretical vertical displacement of a 1-meter section of the 9-5/8" reline casing is 2.04 mm. This calculated displacement is due to thermal expansion alone and it is slightly lower than the simulated value at 2.24 mm. The difference between these two will increase when a longer model is considered because the effect of the contact boundary condition will be more pronounced.

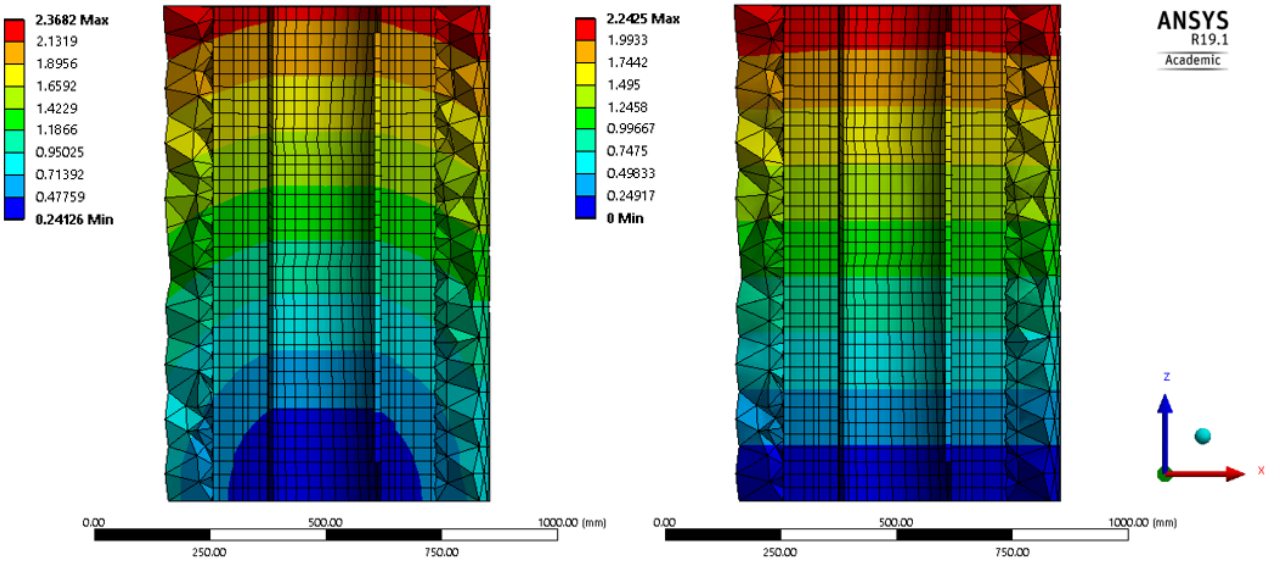

Figure 6: Cross-section of the baseline model showing the total deformation (left) and vertical deformation (right) in mm unit at flowing condition

The details of the models, assumptions, and obtained results for quenching and air compression intervention activities are discussed in the following subsections. The boundary conditions of these models were retained to be identical with the baseline model at operational flowing condition, with the exception of the pressure and temperature loads. Similarly, the simulations of these models were carried out by performing transient thermal analysis and then importing the simulated temperature as a thermal load to the transient structural analysis.

3.1 Quenching

The injecting condition during quenching was estimated using a water loss survey of the well. During the water loss survey, the recorded wellhead pressure was vacuum which indicated that the well had good acceptance. At 20 BPM, the recorded downhole pressure at 2300 meters was at 14.56 MPa. Using this information, the water level during the water loss survey was estimated to be at depth 550 meters, below which the pressure profile is hydrostatic. Since the isolated pit of the model is at depth 19.4 meters, no pressure load was applied to the inner surface of the 9-5/8" reline casing while the temperature load was set at 20 °C based on completion test.

For the initial state of the model, shut condition was considered wherein the pressure and temperature loads are at 0.6 MPa and 158.8 °C, respectively. The well was assumed to be in shut condition for a long time, hence, the initial temperature at 158.8 °C is uniform across the model. Considering a 24-hour duration for the quenching activity, the resulting temperature distributions of the model at different elapsed times are shown in Figure 7. After six hours of continuous cold-water injection, the 9-5/8" reline casing has already cooled down to 20 °C while the outermost concrete remains heated at around 130 °C. The heat continues to be dissipated as time passes by, eventually cooling the outermost concrete at around 90 °C after 12 hours and down to almost 70 °C after 18 hours. Upon reaching the end time, the casing section has significantly decreased in temperature with the outermost concrete at around 50 °C.

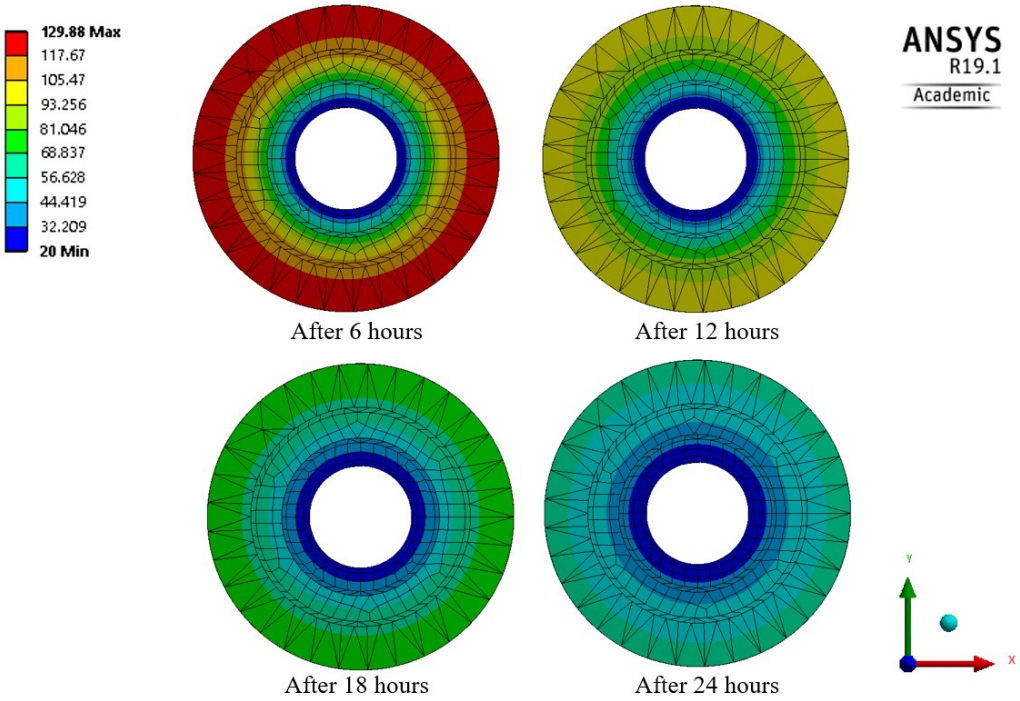

Figure 7: Top view of the model showing the temperature distribution in °C unit at different elapsed times during quenching

The transient analyses involved dynamic response of the bodies and time-dependent loads which resulted to higher stress magnitudes when compared to the results of the baseline model at steady state condition. Shown in Figure 8 are the resulting *von Mises* and maximum principal stress distributions in the model by the end of the 24-hour quenching activity. In both cases, the location of the highest stress value is at the midpoint of the isolated pit. With the maximum *von Mises* stress at 78.22 MPa being less than the assumed ultimate yield strength of steel at 460 MPa, the 9-5/8" reline casing is still safe to operate based on the *von Mises* criterion. However, the maximum principal stress at 80.15 MPa is more than twice the calculated critical value of burst pressure at 45.12 MPa. Without the support of the surrounding concretes and outer casings, there is a high probability that the 9-5/8" reline casing will fail via bursting.

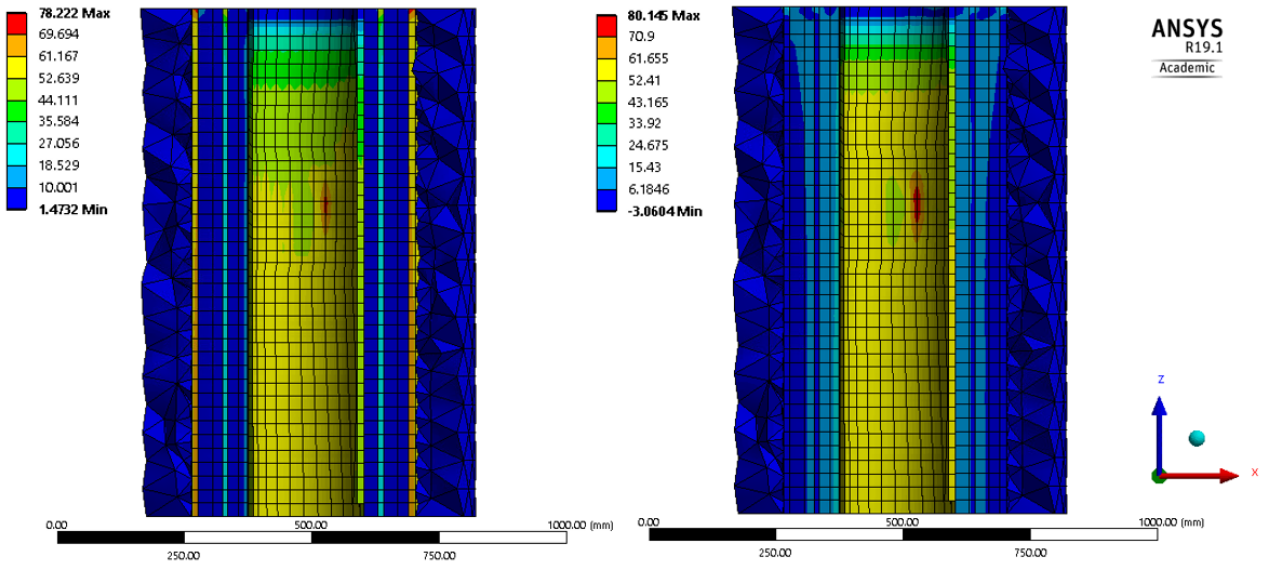

Figure 8: Cross-section view showing the *von Mises* stress (left) and maximum principal stress (right) distributions in MPa unit at the end of quenching

On

3.2 Air Compression

Identical pressure and temperature loads were assumed for the shut condition of the well at 0.6 MPa and 158.8 °C, respectively, as the initial state of the model. The air compression activity that was used as a reference for this analysis lasted for two hours to attain a wellhead pressure of 3.1 MPa. The time-dependent pressure load used in this analysis is based on recorded wellhead pressures of the air compression activity as shown in Figure 9. Inside the casing, the resulting fluid is a mixture of steam and compressed air. For simplicity, the time-dependent temperature load of the model was assumed to be the corresponding saturated steam temperatures of the given pressure load points.

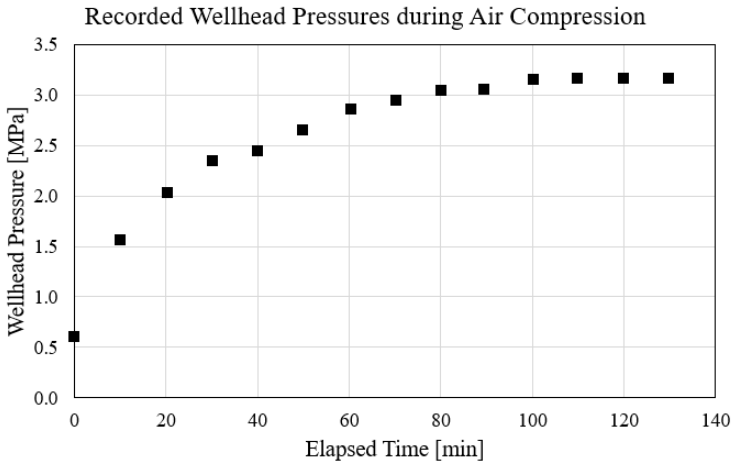

Figure 9: Recorded wellhead pressure of the well during its air compression activity

Considering the 2-hour duration of the air compression activity, the resulting temperature distributions of the model at different elapsed times are shown in Figure 10. The obtained temperature contours show that the outer bodies are less affected by the heat up given the shorter time period. By the end of the activity, the 9-5/8" reline casing has reached a temperature of 236.76 °C while the temperature of the outermost concrete slightly increased at 159.4 °C.

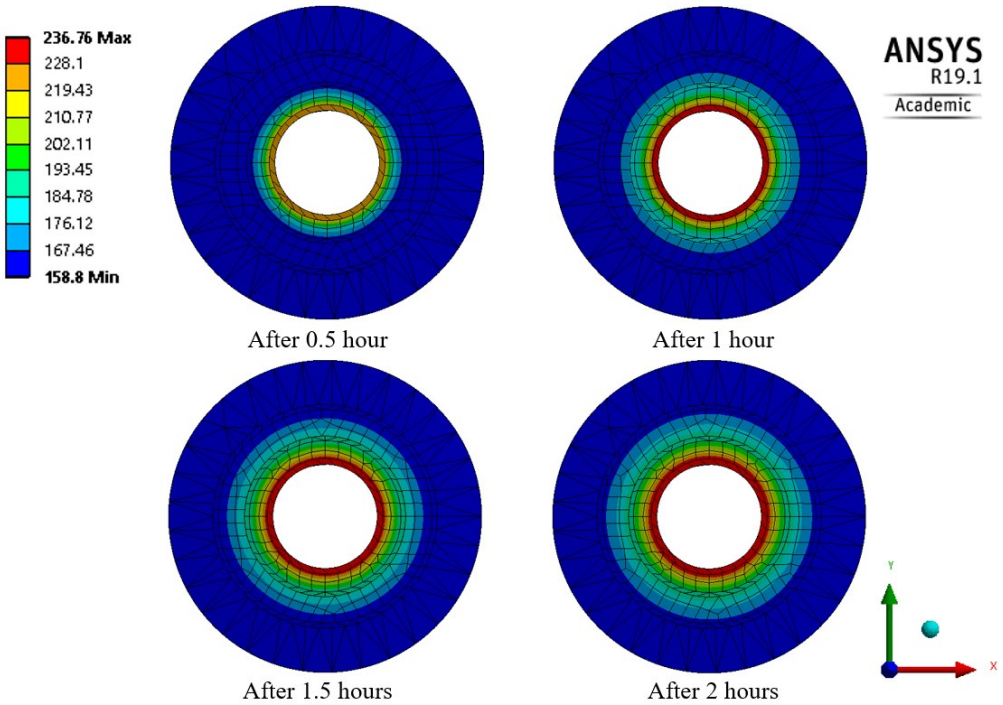

Figure 10: Top view of the model showing the temperature distribution in °C unit at different elapsed times during air compression

The obtained *von Mises* and maximum principal stress distributions by the end of the 2-hour air compression activity are shown in Figure 11. The simulated stress values have higher magnitudes when compared to the other two scenarios because the pressure and temperature loads in air compression are higher. Stress concentration at the isolated pit is evident in the *von Mises* distribution with a corresponding value at 199.49 MPa. This is still less than the assumed ultimate yield strength of steel at 460 MPa, hence, the 9-5/8" reline casing is safe from yielding during air compression. For the maximum principal stress distribution, no stress concentration is depicted at the isolated pit. In this contour, the highest values of the maximum principal stress occur at the upper end of the 18-5/8" anchor casing and 13-13/8" production casing. The obtained maximum principal stresses in the 9-5/8" reline casing are compressive with values around 5 MPa.

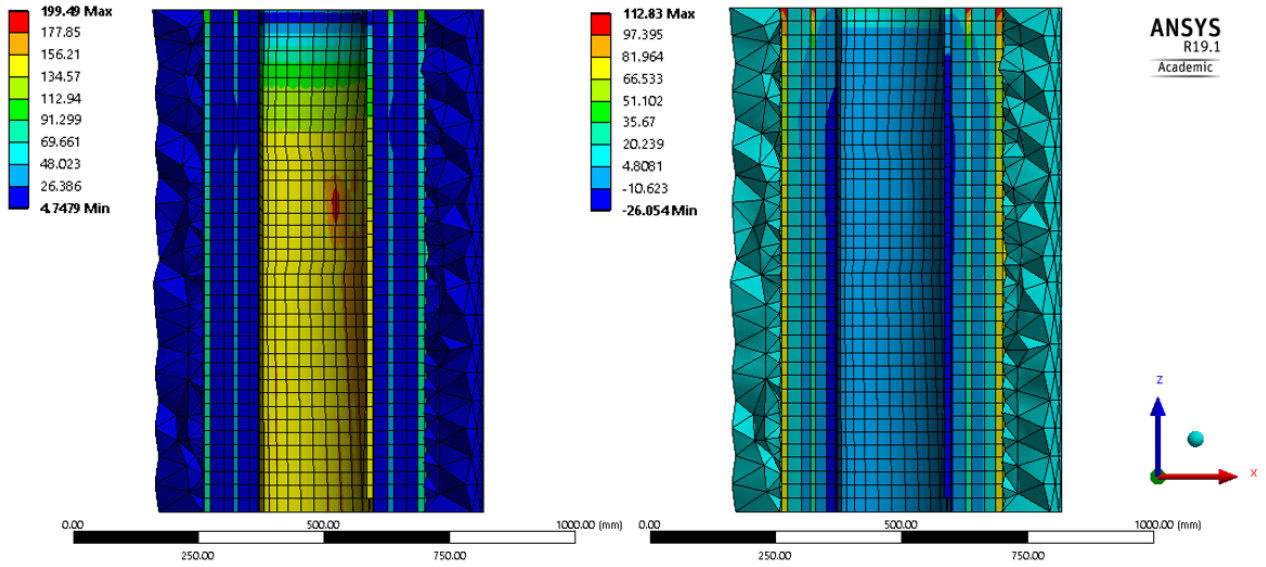

Figure 11: Cross-section view showing the *von Mises* stress (left) and maximum principal stress (right) distributions in MPa unit at the end of air compression

Since the *von Mises* stress is a function of principal stresses, the stress concentration at the isolated pit was found to be evident in the middle principal stress and minimum principal stress distributions as shown in Figure 12. The middle principal stress and minimum principal stress at the midpoint of isolated pit are at 196.18 MPa and 203.38 MPa, respectively, and both of which are compressive. Although the obtained stress magnitudes are high, the 9-5/8" reline casing has less likelihood of bursting given that the principal stresses are compressive.

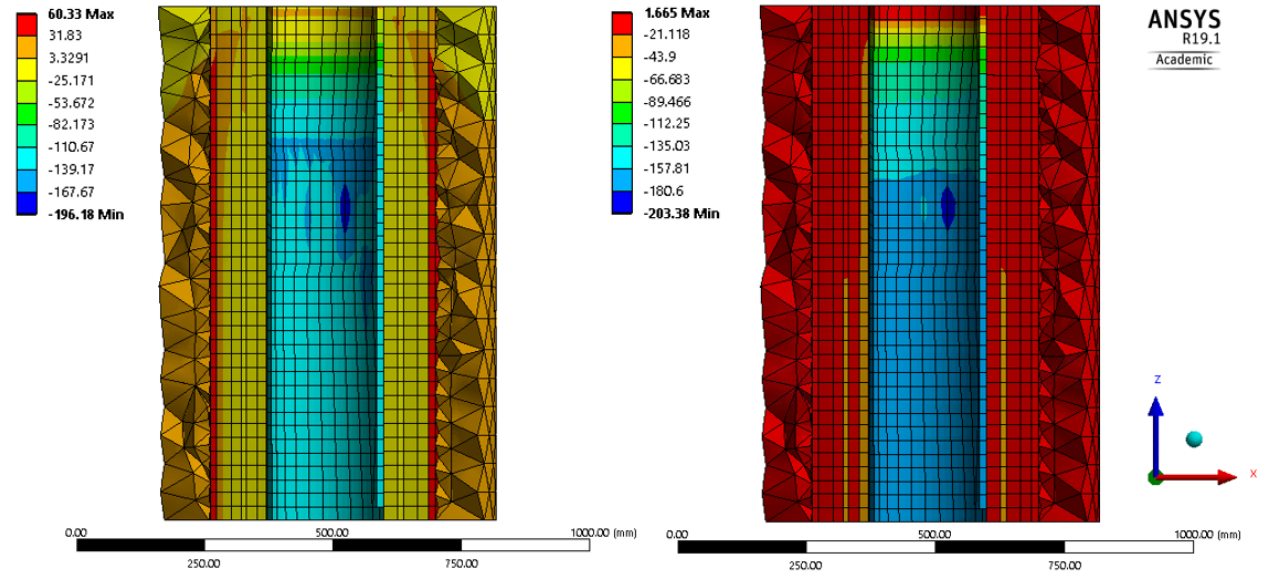

Figure 12: Cross-section view showing the middle principal stress (left) and minimum principal stress (right) distributions in MPa unit at the end of air compression

4. CONCLUSION

A finite element model of a penetrated casing section of a geothermal well presumed to be eroded by the abrasive effects of high-velocity solids has been created using ANSYS® Academic Teaching Mechanical and CFD, Release 19.1. The stress analyses of the penetrated casing model involved simplifications in the boundary conditions such as the use of bonded contact type, elastic support, and other assumptions related to the pressure and temperature loads. Refinements were applied in the mesh design, and a convergence test was conducted to check the balance between numerical accuracy and computational time requirement. Simulation results showed that a stress concentration has developed at the isolated pit of the 9-5/8" reline casing. The casing section was evaluated to be safe from yielding at flowing condition using the *von Mises* criterion. The simulated *von Mises* stress at the isolated pit was found to be 44.85 MPa which is less than the assumed ultimate yield strength of steel at 460 MPa. Identical evaluations were obtained for the quenching and air compression scenarios at 78.22 MPa and 199.49 MPa, respectively. The 9-5/8" reline casing was further evaluated by assessing the risk of burst failure. This was done by comparing the maximum principal stress to its calculated critical burst pressure of 45.12 MPa. The obtained maximum principal stresses for the flowing condition and quenching have exceeded the critical value at 46.6 MPa and 80.15 MPa, respectively. These results indicate that the burst failure of the 9-5/8" reline casing is imminent without the support of the surrounding concretes and outer casings. For the air compression, the principal stresses of the 9-5/8" reline casing were obtained to be compressive suggesting that it has less likelihood of bursting.

On

ACKNOWLEDGEMENT

This project was undertaken during the course of the author's postgraduate study at the University of New South Wales under the financial support of Australia Awards Scholarship and Energy Development Corporation. The author gratefully acknowledges the University for the license privilege to ANSYS® software. The author also recognizes Mr. Phil Howlin, the author's former lecturer, for his invaluable help in sharing his technical expertise in finite element modelling.

REFERENCES

Akbar, S., Fathianpour, N., & Al Khoury, R. (2016). A finite element model for high enthalpy two-phase flow in geothermal wellbores. *Renew. Energy, 94*(C), 223-236. doi:10.1016/j.renene.2016.03.034

ANSYS, Inc. (2018). ANSYS® Academic Teaching Mechanical and CFD, Release 19.1, Help System, Engineering Data User's Guide.

ANSYS, Inc. (2018). Free Software for Students | ANSYS Academic. Retrieved from https://www.ansys.com/academic

Barrett, P. (2015). How to Model Foundation Supports. *CAE Associates - Engineering Advantage Blog.* Retrieved from https://caeai.com/blog/how-model-foundation-supports

Bourgoyne, A. T., Jr., Millheim, K. K., Chenevert, M. E., & Young, F. S., Jr. (1986). *Applied drilling engineering*. Richardson, TX: Richardson, TX, United States: Soc. Pet. Eng.

Buñing, B. C., Sarmiento, Z. F., Aleman, E. T., & Saw, V. S. (2005). *Casing Inspection Caliper surveys: results and implications to operations in Leyte Geothermal Production Field.* Paper presented at the Proceedings World Geothermal Congress 2005.

Christensen, R. M. (2013). *The theory of materials failure*. Oxford: Oxford : Oxford University Press.

Kaldal, G., Jonsson, M., Palsson, H., & Karlsdottir, S. (2015). Structural modeling of the casings in high temperature geothermal wells. *Geothermics, 55*(C), 126-137. doi:10.1016/j.geothermics.2015.02.003

Kurowski, P. (2002). Good Solid Modeling, Bad FEA. Retrieved from https://www.machinedesign.com/fea-and-simulation/good-solid-modeling-bad-fea

Magnúsdóttir, L. (2009). *Nonlinear finite element model of a geothermal well.* (Master of Science). University of Iceland, Reykjavik, Iceland.

Pagli, C., Sigmundsson, F., Lund, B., Sturkell, E., Geirsson, H., Einarsson, P., Hreinsdóttir, S. (2007). Glacio-isostatic deformation around the Vatnajökull ice cap, Iceland, induced by recent climate warming: GPS observations and finite element modeling. *Journal of Geophysical Research: Solid Earth, 112*(B8), n/a-n/a. doi:10.1029/2006JB004421

Pidaparti, R. M. (2017). *Engineering Finite Element Analysis*. San Rafael, California: Morgan & Claypool.

Southon, J. N. (2005). *Geothermal well design, construction and failures.* Paper presented at the Proceedings World geothermal congress.